Eur. J. Mineral.
2013, **25**, 255–266
Published online April 2013

Paper presented at the EMPG XIV symposium, Kiel, Germany (March 2012)

Kinetics and dynamics of mass-transfer-controlled mineral and bubble dissolution or growth: a review

YOUXUE ZHANG

Department of Earth and Environmental Sciences, the University of Michigan, Ann Arbor, MI 48109, USA
*Corresponding author, e-mail: Youxue@umich.edu

Abstract: In geology and daily life, kinetics and dynamics of particle (including crystal, droplet, and bubble) dissolution or growth in a liquid are a large class of often-encountered problems. The growth or dissolution of bubbles and drops are usually controlled by mass transfer, whereas the growth or dissolution of crystals may be controlled either by mass or heat transfer or by interface reaction. In this paper, recent advances in kinetics and dynamics of particle dissolution or growth controlled by mass transfer are reviewed, focusing on quantitative prediction models. Mass-transfer-controlled growth or dissolution can be further distinguished as diffusive (non-convective) or convective. For both types of particle dissolution or growth, approximate models are available for not only a single particle, but also multiple particles. These models have no free parameters. Hence, dissolution or growth rates can be calculated as long as the relevant physical and chemical properties are known, including: diffusivity in the liquid, viscosity of the liquid, and saturation condition between the particle and the liquid.

Key-words: mass-transport control, crystal dissolution, crystal growth, bubble growth, droplet growth, droplet dissolution.

1. Introduction

Thermodynamics deals with the equilibrium state, and kinetics treats the mechanism and rate to reach the equilibrium state. For many geological systems, the thermodynamics has been studied for a long time and is understood fairly well, but the kinetics is not. Examples include processes such as magma crystallization upon cooling, magma degassing upon decompression, and liquid immiscibility.

Thermodynamics of magma crystallization has been investigated for about 100 years (at least from Bowen, 1914), and it is now possible to predict (with increasingly high accuracy) the crystallization temperature and sequence (*e.g.*, MELTS program, Ghiorso *et al*., 2002). On the other hand, experimental mineral growth and dissolution rates have only been studied for about 30 years (*e.g.*, Watson, 1982), and quantification and prediction of mineral dissolution rates in silicate melts became available only recently (*e.g.*, Zhang *et al*., 1989; Kerr, 1995; Liang, 1999, 2000; Zhang & Xu, 2003; Chen & Zhang, 2008, 2009).

The thermodynamics of magma degassing (the solubility of H_2O in natural silicate melts), a critical aspect in explosive volcanic eruptions, has been investigated for a long time (*e.g.*, Goranson, 1938; Tuttle & Bowen, 1958; Shaw, 1963), whereas the kinetics and dynamics of magma degassing (bubble nucleation and growth in oversaturated melts) have only been quantitatively modeled and experimentally studied in the last 20 years (Proussevitch *et al*., 1993; Huwitz & Navon, 1994; Lyakhovsky *et al*., 1996; Navon *et al*., 1998; Proussevitch & Sahagian, 1998; Gardner *et al*., 1999, 2000; Liu & Zhang, 2000; Blower *et al.*, 2002; Gardner & Denis, 2004; Larsen & Gardner, 2004; Lensky *et al*., 2004; Gardner, 2007; Larsen, 2008). Now bubble growth rates can be calculated from solubility, diffusivity and viscosity data in many instances without free fitting parameters, but bubble nucleation rates still rely on experiments.

A third example is immiscibility and separation of sulfide liquid or monosulfide solid solution from silicate melt, a key process in the formation of magmatic sulfide ore deposits. The equilibrium solubility of sulfide phases in silicate melt has been investigated extensively over the years (*e.g.*, Naldrett, 1969; Haughton *et al*., 1974; Shima & Naldrett, 1975; Buchanan & Nolan, 1979; Carroll & Rutherford, 1987; Luhr, 1990; Peach & Mathez, 1993; Gaetani & Grove, 1997; Mavrogenes & O'Neill, 1999; Holzheid & Grove, 2002; O'Neill & Mavrogenes, 2002; Bockrath *et al*., 2004; Jugo *et al*., 2005a, and b; Moretti & Ottonello, 2005; Barnes, 2007; Liu *et al*., 2007; Kress *et al*., 2008; Moretti & Baker, 2008; Jugo, 2009; Li & Ripley, 2009; Baker & Moretti, 2011; Beermann *et al*., 2011; Botcharnikov *et al*., 2011). On the other hand, the kinetics and dynamics of sulfide phase formation, growth, and sinking to form ore deposits have not been quantified yet (Holzheid, 2010, dealt with the separation of sulfide melt droplets from silicate melt).

Many geological processes are non-equilibrium processes and hence the kinetics and dynamics can be critical in understanding them. For example, during gas-driven volcanic eruptions, bubble nucleation and growth kinetics plays

DOI: 10.1127/0935-1221/2013/0025-2292

0935-1221/13/0025-2292 $ 5.40

a major role in the eruption dynamics before magma fragmentation. In igneous rocks, crystallization kinetics controls the extent of crystallization and the size of the crystals as a function of cooling rates. In champagne, kinetics of bubble nucleation and growth determine whether the bottle of champagne would erupt upon opening. In sulfide-bearing magmas, the kinetics and dynamics of sulfide phase formation and sinking likely control whether magmatic sulfide ores would form (Holzheid, 2010).

Mineral/drop/bubble dissolution or growth all belong to a class of problems, which I will refer to as particle dissolution or growth in a liquid, where the ''particle'' can be either a crystal, a drop, or a bubble. This class of problems is often encountered in geology, engineering, and daily life. Furthermore, in daily life, there is a lot of kinetic ''fizzics'' in beer and champagne, including bubble nucleation, bubble growth, bubble coalescence, formation of a foam, and foam stability (*e.g.*, Shafer & Zare, 1991; Liger-Belair, 2002; Zhang & Xu, 2008). This paper reviews the kinetics and dynamics of particle growth or dissolution controlled by mass transfer.

Growth and dissolution occur because there is disequilibrium. Growth of a new phase means that the new phase is more stable, and vice versa. The disequilibrium condition can arise due to change in temperature, pressure or other conditions. For example, bubble growth often occurs when pressure decreases, *e.g.*, due to magma ascent or opening of a bottle of champagne. Crystallization of a magma occurs when there is temperature decrease or water loss. Partial melting occurs when there is pressure decrease (at mid-ocean ridges), or addition of water (at subduction zones), or temperature increase.

In the general sense, when one phase grows, the other phase dissolves. That is, dissolution and growth are opposite processes involving similar principles. However, there can also be differences in treating them. The definition of dissolution means that both phases (different compositions) are already present, and no nucleation is needed. On the other hand, the term ''growth'' may have some ambiguity. It may mean either to start from a liquid phase without the new phase being present initially, in which case nucleation is the first step for crystal growth; it may also mean post-nucleation growth. In this work, the term ''growth'' refers to post-nucleation growth. With this narrower definition of growth, drop and bubble growth can be treated using the same principles as drop and bubble dissolution, but crystal growth may still be slightly different from crystal dissolution in at least two aspects: (i) during crystal dissolution, the crystal composition essentially stays the same as the initial crystal composition (but see Zhang, 2008, pp. 382–387 for more details), but during crystal growth, the newly grown crystal composition depends on the interface melt composition, and (ii) when the degree of oversaturation is very high and diffusion is slow, there may be dendritic growth, but dendritic dissolution is not observed though dendritic partial melting has been reported and explained (Tsuchiyama & Takahashi, 1983; Zhang, 2008, pp. 361–362). Hence, one needs to assess case by case whether crystal growth can be treated using crystal dissolution theory.

2. Controlling mechanisms of particle dissolution or growth

Mineral growth and dissolution may be controlled either by biological processes or inorganic processes. Examples of biological control include the formation and growth of calcium carbonate in corals, which often show ''vital'' effects due to the ability of organisms to alter the local environment (such as ionic concentrations). Biologically controlled growth or dissolution is not the subject of this work; only inorganic growth or dissolution is considered in this work.

In crystal growth or dissolution, two sequential steps are required. One is interface reaction, which is the attachment or detachment of atoms/ions to or from the crystal surface. It is expected that when solubility is small or when strong bonds must be broken, interface reaction is slow. Otherwise, it is rapid. The other is mass transport (or mass transfer) to and from the crystal surface. For crystal growth, nutrient (compatible) components must be transferred to the crystal surface, and incompatible components that pile up at the crystal surface must be transferred away. The lower limit of mass transfer (in the absence of convection) is controlled by diffusion. In aqueous solutions at room temperatures, the diffusion coefficients of most species are similar (of the order of 1×10^{-9} to 2×10^{-9} m^2/s, Cussler, 1997, p. 112). Because interface reaction and mass transfer are sequential steps during particle growth and dissolution, the slowest step (bottleneck) determines the overall rate. Hence, when solubility is small and bonds are strong, it is expected that interface reaction is slow and will control the dissolution since diffusion rates do not vary much. Berner (1978) summarized and interpreted literature data on mineral dissolution in aqueous solutions, and Zhang (2008) reinterpreted the data (Fig. 1), consistent with this expectation. According to Fig. 1, whether the dissolution of a mineral is

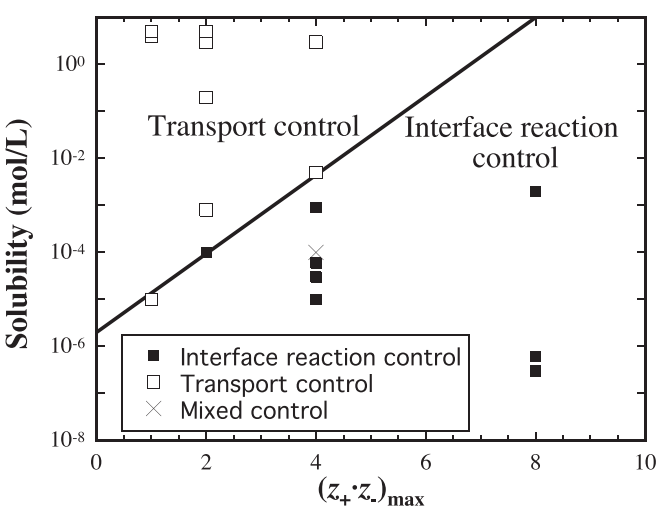

Fig. 1. Control of mineral dissolution in aqueous solution. z_+ and z_- are the valences of the cation and anion to be separated during dissolution. Data are from Berner (1978). The solid line separates the region between transport control and interface reaction control. From Zhang (2008).

controlled by interface reaction or by mass transfer is influenced by two factors: one is solubility, and the other is bond strength. The higher the solubility, the more need for mass transfer, and hence the process is more likely controlled by mass transfer. On the other hand, the stronger the bond, the slower the interface reaction rate, and the process is more likely controlled by interface reaction. Hence, as shown in Fig. 1, for minerals with high solubility and weak bonds, the dissolution is controlled by mass transport. Otherwise, it is controlled by interface reaction.

Operationally, interface control means that the interface liquid composition is the same as the far-field composition, whereas transport control means that the interface liquid composition is roughly the saturation composition and different from the far-field composition (Zhang, 2008, p. 51). If the interface liquid composition varies with time from the far-field composition to the saturation composition, then the process is controlled by both interface reaction and transport.

For bubble and drop dissolution or growth in water or in melt, the interface reaction rate is expected to be high because molecules in most liquid and gas can be removed or added without a significant energy barrier. Hence, although to the author's knowledge no one assessed the control mechanism of bubble and droplet growth or dissolution, it is generally assumed that mass transport controls the overall dissolution or growth rate in both aqueous solutions and in silicate melts (*e.g.*, Epstein & Plesset, 1950; Scriven, 1959; Sparks, 1978; Proussevitch & Sahagian, 1998; Zhang, 2005). The success of these models in predicting experimental data (see below) may be viewed as a verification that bubble and drop dissolution and growth are indeed controlled by mass transfer.

In magmatic systems, no systematic study on the control of mineral dissolution mechanism has been carried out. Earlier studies (*e.g.*, Watson, 1982; Harrison & Watson, 1983) often implicitly assumed that mineral dissolution is mass transfer controlled. In non-convective systems, this means diffusion control. Zhang *et al.* (1989) analyzed numerically the role of interface reaction and diffusion for non-convective crystal dissolution. They found that as time increases, the dissolution gradually becomes diffusion controlled, and the time for crystal dissolution to become diffusion controlled depends on the ''reduced'' dissolution rate V_a (dissolution rate at a fixed degree of undersaturation, *e.g.*, interface melt concentration of zero), as well as the diffusivity, the initial degree of saturation, and the crystal composition. For the case of non-convective diopside dissolution, diffusion control is reached in less than 1 s. Although the parameter V_a was not known for other minerals, Zhang *et al.* (1989) concluded that if the values of V_a for other minerals are comparable to that for diopside (which needs more investigation), dissolution would be essentially diffusion controlled. Experiments of Zhang *et al.* (1989) and Chen & Zhang (2008, 2009) demonstrate that non-convective olivine and clinopyroxene dissolution is controlled by diffusion rather than interface reaction. Morgan *et al.* (2006) showed that non-convective dissolution of plagioclase is controlled by diffusion.

There are also studies that indicate the interface melt composition depends on time during non-convective mineral dissolution in silicate melts, suggesting that the dissolution is controlled by both interface reaction and diffusion. Shaw (2000) showed that during quartz dissolution in basanite melt, SiO_2 concentration in the interface melt evolves from about 60 wt% at experimental heating time (t) = 20 min to about 73 wt% at t = 4.5 hr. Shaw (2004, 2006) further showed that during quartz dissolution in CMAS melts, SiO_2 concentration in the interface melt also changes with time. Acosta-Vigil *et al.* (2002, 2006) studied dissolution of corundum, andalusite, albite and orthoclase in haplogranitic melts at 800°C and also found that the interface melt composition evolves from the initial melt composition gradually to the saturation melt composition. These studies indicate that the dissolution of some minerals is controlled by both interface reaction and mass transport. For dissolution of minerals in silicate melts, no case of pure interface control (meaning that the interface melt composition is the same as the far-field melt and stirring or convection would not enhance the dissolution rate; Zhang, 2008) has been reported. It is possible that stronger bonds in the crystals mean that interface reaction is slow and hence is more likely to play a role in controlling crystal dissolution in silicate melts, similar to the case of mineral dissolution in aqueous solutions. A systematic study of the dissolution behavior of different minerals in various melts at some given temperatures and pressures is necessary to characterize the behavior using both experimental data and numerical analysis.

When interface reaction controls dissolution or growth, the reaction rate depends on the detailed reaction mechanism and the crystal may display anisotropic dissolution behavior. On the other hand, when mass transfer controls dissolution or growth, the rate can be quantified by considering mass transfer in the liquid and interface equilibrium, and there is no anisotropy. The transfer-controlled dissolution or growth have been quantified in several cases in recent years, and are the focus below.

3. Transport-controlled dissolution or growth

Transport-controlled dissolution or growth can be further classified as diffusion control and convection control. In diffusive control (Fig. 2), the growing or dissolving particle does not move buoyantly relative to the liquid, and there is not enough Rayleigh instability for the interface liquid layer to rise or sink freely through the rest of the liquid. This typically occurs when the viscosity of the liquid is high, such as bubble growth/dissolution or crystal growth/dissolution in rhyolitic melt. The compositional boundary layer in the case of diffusion control gradually thickens (Zhang, 2008), but a limit may exist in 3-dimensional cases (Carslaw & Jaeger, 1959, p. 232).

When liquid viscosity is low, the particle may sink or rise buoyantly (*e.g.*, bubble growth in beer). Such motion induces convection in the liquid, which partially removes the diffusive boundary layer. This situation is referred to as

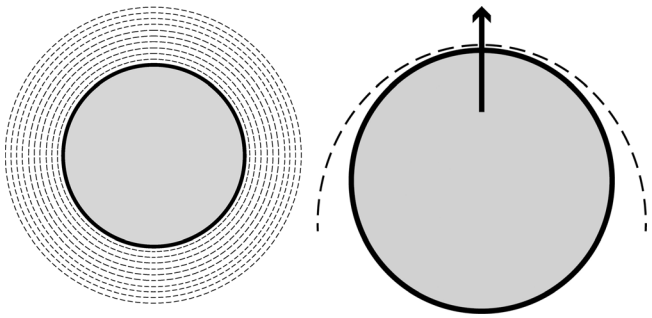

Fig. 2. Shapes of boundary layer for diffusive (left-hand side) and convective (right-hand side) particle growth or dissolution. The particle is bounded by the heavy solid circle in each case. For diffusive particle growth or dissolution, the dashed circles represent gradual thickening of the boundary layer. For convective growth or dissolution of a rising particle, the dashed curve shows the leading side of the boundary layer at steady state. On the trailing side, the boundary layer approaches infinite thickness.

forced convection and is depicted in Fig. 2. Convection may also arise because the liquid adjacent to the growing or dissolving particle has different densities, which may cause the interface liquid to rise or sink with or without particle motion, thinning the compositional boundary layer. This situation is referred to as free convection. Forced convection is often more important than free convection (Kerr, 1995; Zhang & Xu, 2003). The operation of convection often reaches steady state, at which the effective boundary layer thickness becomes time independent at constant particle size. In the case of forced convection, reaching the steady-state boundary layer is similar to reaching the terminal velocity of the moving particle. The mean time to reach the terminal falling or rising velocity for a rigid spherical particle in a fluid in the Stokes' flow regime can be estimated as $2a^2\rho/(9\ \eta)$ where a and ρ are the radius and density of the moving particle, and η is the viscosity of the ambient fluid (Wang & Pruppacher, 1977). For example, for the dissolution of a 0.1-mm-diameter NaCl crystal in water, the mean time to reach the terminal velocity is 0.0012 s, which is shorter than the mean time needed for diffusion to establish the effective boundary layer (estimated from δ^2/D where δ is the boundary layer thickness and D is the diffusivity). Hence, the mean time needed to reach the terminal velocity is short and is not limiting the application of steady-state treatment theories, which is an advantage because no theory has been advanced yet to tackle growth or dissolution with non-steady-state convection. When either forced convection or free convection is present, mass transfer is enhanced. The growth or dissolution will be referred to as convective growth or dissolution, even though mass transfer through the boundary layer is still by diffusion.

Prior to 1989, most authors studying mineral dissolution did not clearly distinguish diffusive *versus* convective dissolution. Zhang *et al*. (1989) pointed out the importance of distinguishing diffusive and convective crystal dissolution, and investigated diffusive crystal dissolution. Kerr (1995) introduced convective dissolution theory to the geological community for cases of $\mathrm{Re} \leq 1$. Zhang & Xu (2003) expanded the treatment to cases of $\mathrm{Re} \leq 10^5$.

4. Diffusive bubble growth in rhyolitic melt

Epstein & Plesset (1950), Scriven (1959) and Sparks (1978) modeled diffusive growth of an individual stationary bubble in liquid and obtained approximate solutions. Major progress on bubble growth was made by Proussevitch, Sahagian and coworkers. Proussevitch *et al*. (1993) set up the framework for modeling growth of many stationary bubbles with periodic alignment (Fig. 3) in a melt containing one gas component. In this model, the viscosity of the liquid and the diffusivity of the gas component in the liquid are assumed to be independent of concentration (which depends on the distance from bubble wall). The model is useful in terms of examining the effect of various parameters, but is not practical for predicting H_2O bubble growth in silicate melts because it is known that both viscosity and H_2O diffusivity depend strongly on H_2O concentration in the melt (Shaw, 1972, 1974; Delaney & Karsten, 1981; Zhang & Stolper, 1991; Zhang *et al*., 1991a and b; Hess & Dingwell, 1996). In a major improvement, Proussevitch & Sahagian (1998) upgraded the multi-bubble growth model for variable viscosity and diffusivity, allowing for realistic bubble growth modeling in silicate melts. The main parameters controlling bubble growth rates are: melt viscosity (depending on temperature, melt composition, and H_2O content), gas solubility (depending on temperature, gas pressure, and melt composition) and gas component diffusivity (depending on temperature, H_2O content, pressure and dry melt composition) in the melt. Surface tension (Walker & Mullins, 1981) also plays some role for small bubbles. Melt density (Lange & Carmichael, 1990; Ochs & Lange, 1997) and gas phase density are also necessary input parameters. There are also bubble growth models for more specific situations (*e.g*., Navon *et al*., 1998), which are not covered here.

The H_2O bubble growth model of Proussevitch & Sahagian (1998) in silicate melts is summarized below. A bubble in a multi-bubble ''lattice'' is simplified as a bubble growing in a melt shell (Fig. 3). The bubble radius is denoted as a (depending on time), and the melt shell is from $r = a$ to $r = b$ with shell thickness of b–a (Fig. 3; see also Fig. 1 in Proussevitch & Sahagian, 1998). The

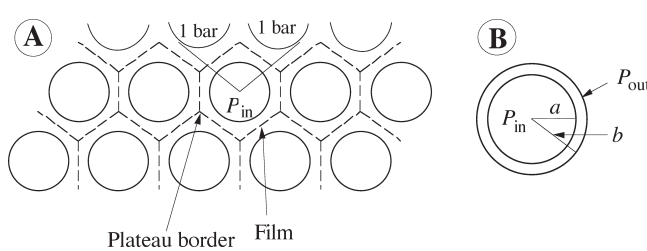

Fig. 3. Sketch for the simultaneous growth of multiple equal-sized bubbles. A shows the hypothetical arrangements of the bubbles. B shows further simplification for the growth of an individual bubble. From Proussevitch & Sahagian (1998) and Zhang (1999a).

diffusion equation in the reference frame fixed at the bubble center is:

$$\frac{\partial w}{\partial t} = \frac{1}{r^2}\frac{\partial}{\partial r}(Dr^2\frac{\partial w}{\partial r}) - u\frac{a^2}{r^2}\frac{\partial w}{\partial r}, t > 0, a < r < b, \quad (1)$$

where w is H_2O mass fraction in the melt, D is total H_2O diffusivity in the melt (depending on H_2O concentration in rhyolitic melt; *e.g.*, Ni & Zhang, 2008) and u is bubble growth rate:

$$u = \mathrm{d}a/\mathrm{d}t. \quad (2)$$

To solve Equation (1), in addition to knowing the dependence of D as a function of H_2O content (using H_2O diffusivity model available at the time), the initial and boundary conditions must be given, and a and b must be obtained (then u can be obtained as $\mathrm{d}a/\mathrm{d}t$). The initial condition is typically uniform concentration in the melt: $w|_{t=0} = w_0$. Two boundary conditions are:

$$w|_{r=a} = f(T, P_g) = \text{Solubility relation}, \quad (3)$$

$$\left.\frac{\partial w}{\partial r}\right|_{r=b} = 0, \quad (4)$$

where P_g is the pressure in the bubble and can be found as follows:

$$P_g = P_f + \frac{2\sigma}{a} - 4ua^2\int_{z(a)}^{z(S)}\eta(z)dz, \quad (5)$$

where P_f is the pressure on the ambient melt, σ is surface tension, η is melt viscosity (depending on H_2O content, and hence depending on r value), $z = 1/r^3$, $2\sigma/a$ is the pressure due to surface tension, and the last term on the right-hand side is additional bubble pressure that pushes the viscous melt away so that the bubble can grow. The above equation applies to the case of uniform temperature in the region of bubble growth. (The case for temperature change with time can be incorporated in the model, Proussevitch & Sahagian, 1998.) The fact that hydrous rhyolitic melt viscosity depends strongly on H_2O content makes the last term a complicated integral.

The bubble radius a can be found from mass balance at the bubble-melt interface assuming ideal gas law:

$$\frac{\mathrm{d}}{\mathrm{d}t}\left(\frac{4\pi a^3 P_g}{3RT}\right) = \frac{1}{M}4\pi a^2 D\rho_m\left.\frac{\partial w}{\partial r}\right|_{r=a}, \quad (6)$$

where R is the gas constant, M is the molecular mass of H_2O, and ρ_m is melt density. Because P_g in the above equation depends on a, Equations (2), (5) and (6) must be solved simultaneously for a, P_g, and u.

Finally, b can be found as follows assuming constant density for the melt (the melt is losing some mass to the bubble):

$$(b^3 - a^3) + \frac{1}{\rho_m}(\rho_g a^3 - \rho_{g,0}a_0^3) = (b_0^3 - a_0^3), \quad (7)$$

where a_0 and b_0 are the initial values of a and b, ρ_g and $\rho_{g,0}$ are the gas density in the bubble at time t and time 0.

For realistic modeling of bubble growth, realistic relations for solubility, diffusivity and viscosity for a given melt must be used. They are from available models in the literature for specific melts.

Liu & Zhang (2000) conducted bubble growth experiments in rhyolitic melt at 500–600°C and 0.1 MPa to test the accuracy of the bubble growth model of Proussevitch & Sahagian (1998) using available solubility, viscosity, and diffusivity models. The solubility of H_2O in rhyolitic melt as a function of temperature and H_2O pressure was already well known by then (*e.g.*, Shaw, 1963; Kadik *et al*., 1972; Khitarov & Kadik, 1973; Dingwell *et al*., 1984; Silver *et al*., 1990; Ihinger, 1991; Holtz *et al*., 1992, 1995; Blank *et al*., 1993; Moore *et al*., 1995, Moore *et al*., 1998; Zhang, 1999b), with only small differences between different models in the 1990s (with exception of some simple linear regressions, see discussion in Zhang *et al*., 2007). The solubility model in Zhang (1999) was chosen by Liu & Zhang (2000). Viscosity models for hydrous rhyolitic melt are limited, especially at temperatures of 500–600°C. The earlier model by Shaw (1972) cannot be applied to such low temperatures. Hence, the non-Arrhenian viscosity model for hydrous rhyolitic melt by Hess & Dingwell (1996) was used. For H_2O diffusivity, the model by Zhang & Behrens (2000) was employed. The calculated results are shown as dashed curve in Fig. 4, with experimental data shown as points. There is significant mismatch (often a factor of 2–4 in the growth rate) between the calculation and the experimental data. Because there is no free parameter in the calculation, agreement within a factor of 2–4 is not that bad. Nonetheless, it is important to determine whether the disagreement is due to inadequacy in the bubble growth model, or due to uncertainty in the input parameters (*i.e.*, models) for viscosity, diffusivity, and solubility. Because (i) solubility is known well, (ii) the uncertainty in the diffusivity is no more than 50%, and (iii) the viscosity model of Hess & Dingwell (1996) has a stated 2σ uncertainty of a factor of 8, simulations by Liu & Zhang (2000) show that the disagreement is most likely due to uncertainty in the viscosity model of Hess & Dingwell (1996).

Zhang *et al*. (2003) developed a new viscosity model for hydrous rhyolitic melts. They assumed that viscosity values from bubble growth experiments assuming the growth model of Proussevitch & Sahagian (1998) are accurate, and used these values to calibrate the ''hydrous-species-reaction viscometer''. Using this hydrous-species-reaction viscometer, they inferred viscosity values from controlled cooling rate experiments, and combined these data with literature viscosity data to construct a new viscosity model for hydrous rhyolitic melts. Although calculated bubble growth curves match experimental data well using the new viscosity model of Zhang *et al*. (2003), this fact, in itself, is not enough to demonstrate that bubble growth rates can be calculated using the model of Proussevitch & Sahagian (1998) due to circularity of argument (because viscosity calibration assumed that the model of Proussevitch & Sahagian, 1998 was accurate). Recently, Hui *et al*. (2009) compared directly measured viscosity using parallel plate method with viscosity inferred from the ''hydrous-species-reaction viscometer''

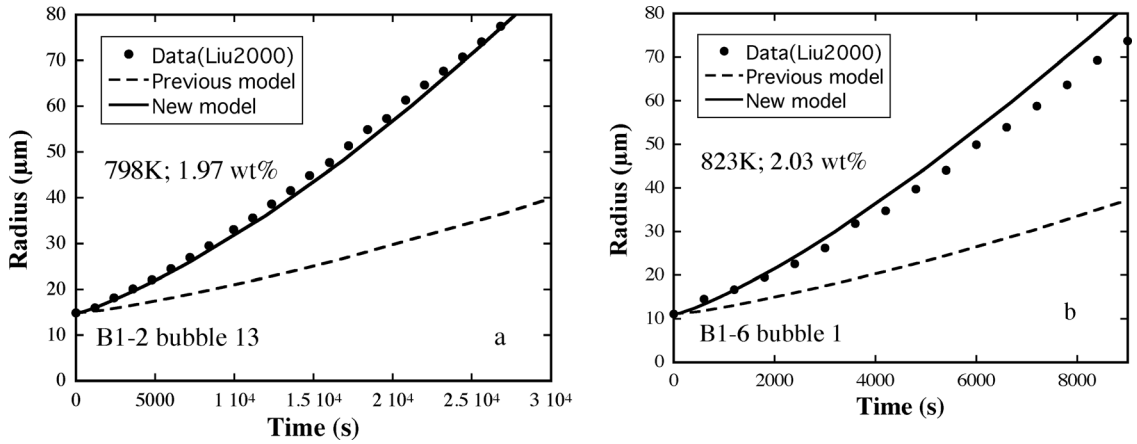

Fig. 4. Diffusive bubble growth, comparison of experimental data and model calculations. Dashed curves used the viscosity model of Hess & Dingwell (1996); and solid curves used the viscosity model of Zhang *et al*. (2003).

and found that the two data sets at 575–650°C are in excellent agreement (within 0.08 log units and with negligible systematic difference). Therefore, it can be regarded now that viscosity values inferred from the ''hydrous-species reaction viscometer'' are calibrated against the physically measured viscosity data rather than data from bubble growth experiments by assuming the model of Proussevitch & Sahagian (1998) is accurate. That is, it can now be regarded that the viscosity model of Zhang *et al*. (2003) is independent of the bubble growth model of Proussevitch & Sahagian (1998), and therefore can be utilized to test the accuracy of the latter.

The H_2O diffusivity model of Zhang & Behrens (2000) has also been improved slightly by Ni & Zhang (2008), especially with respect to the pressure effect. Because most diffusion data were obtained at high pressures, and bubble growth experiments were conducted at 0.1 MPa, the better constrained pressure effect allows more accurate estimation of diffusivity at 0.1 MPa.

Using the new viscosity model of Zhang *et al*. (2003) as verified by Hui *et al*. (2009) and the diffusivity model of Ni & Zhang (2008) as input parameters, calculated bubble growth curves are shown as solid curves and compared with bubble growth data in Liu & Zhang (2000) in Fig. 4. The agreement is excellent. Calculations for more bubble growth data show that the agreement is typically within 20%. Liu & Zhang (2000) also showed that the bubble growth data during continuous decompression (Gardner *et al*., 1999) are roughly consistent with calculations using the model of Proussevitch & Sahagian (1998). Other bubble growth data by continuous decompression experiments, which became available later (*e.g.*, Larsen & Gardner, 2004), are also in qualitative agreement with the model of Proussevitch & Sahagian (1998) although quantitative verification cannot be made due to lack of H_2O diffusion data in the specific melts. In summary, the diffusive bubble growth model of Proussevitch & Sahagian (1998) is realistic enough to predict diffusive bubble growth rates as long as accurate solubility, viscosity and diffusivity models are available for the melt.

The model described in this section can easily treat diffusive growth or dissolution of a single bubble in an infinite melt: by letting $b \rightarrow \infty$. Furthermore, with some minor changes, the method can also be modified to deal with diffusive growth and dissolution or many equal-sized droplets or crystals of the same kind (*e.g.*, many equal-sized olivine grains). The problem of diffusive growth or dissolution of different-sized particles has not been solved yet, nor is the case of many interacting grains of different crystals (such as many olivine, pyroxene and plagioclase grains).

5. Convective CO_2 drop dissolution in seawater

For convective particle growth and dissolution, dissolution of rising CO_2 drops in seawater is discussed first. In order to mitigate global warming, several proposals have been made to reduce emission of CO_2 into the atmosphere. One is to collect CO_2 from power plants, liquefy it, and inject the liquid CO_2 into ocean water. To evaluate the feasibility of such injection, it is necessary to know what would happen to the injected CO_2 liquid. CO_2 liquid density depends strongly on pressure (Angus *et al*., 1976). In oceans at $\geq$2000 m below sea level, CO_2 liquid is usually denser than seawater, and CO_2 liquid would sink toward ocean bottom. At $\leq$1000 m below sea level, CO_2 liquid is usually less dense than seawater, and CO_2 liquid would rise toward the surface. Between 1000–2000 m, the density difference is small and which phase is denser depends on other factors such as salinity and temperature. To minimize cost, it is desirable to inject into shallower depth. Hence, experiments have been carried out for injection depth of about 600 m.

Brewer *et al*. (2002) investigated the fate of injected CO_2 liquid in seawater. They used a remotely operated vehicle (ROV) carrying liquid CO_2, injection device, and a HDTV camera. At a depth of 600–800 m below sea level, liquid CO_2 is injected in seawater by the ROV. The injected liquid CO_2 breaks into drops in seawater, and the drops rise toward the surface in the experiments. They tried to move the ROV at the same speed as the rising drops,

taking videos of the drops and measuring the size of the drops from the videos. It takes trials and errors to get the ROV to follow the drops successfully and obtain useful data. Brewer *et al*. (2002) reported data for the rise and dissolution of two drops, one of which was followed from 800 m depth, and the other followed from 650 m depth. The depth and radius of each drop were measured as a function of time, as well as the local temperature.

Convective particle dissolution theory has been introduced by Kerr (1995) and Zhang & Xu (2003). One additional complexity specific for the dissolution of CO_2 drops is the formation of a thin hydrate shell at the interface between CO_2 liquid and water because CO_2 hydrate is more stable than CO_2 liquid plus water in the temperature and pressure condition of seawater in which CO_2 drops were rising and dissolving. The formation of this shell has been confirmed by Brewer *et al*. (2002), and it has the following consequences:

(1) The liquid drop with the thin shell can be treated as a rigid sphere, even though the bulk of the drop plus the shell is still liquid. This simplifies the theory for the rise and dissolution of CO_2 drops.
(2) The solubility of hydrate shell is smaller than the solubility of CO_2 liquid in seawater, meaning that the formation of the hydrate shell makes the CO_2 drop more stable.

During particle dissolution or growth, the liquid composition at the particle-liquid interface is different from the far-field liquid composition. The liquid layer adjacent to the growing or dissolving particle through which the composition varies from the interface composition to the far-field composition is referred to as the boundary layer. The mathematical definition of the compositional boundary layer thickness δ is:

$$\delta = \frac{w_\infty - w_a}{(\partial w/\partial r)_{r=a}}, \tag{8}$$

where a is particle radius, $r = a$ is at the particle-liquid interface, w_a and w_∞ are mass fraction of the particle component in the interface and far-field liquid respectively. This definition applies for both diffusive and convective particle dissolution or growth. For the growth or dissolution of a falling or rising spherical particle, the compositional boundary layer thickness actually varies with direction: being thinnest at the leading side and thickest at the trailing side (Fig. 2). The above defined boundary layer thickness is hence the effective boundary layer thickness.

For the growth or dissolution of a falling or rising spherical crystal or drop controlled by mass transfer, based on mass balance, the linear growth or dissolution rate can be written as (Kerr, 1995; Zhang & Xu, 2003):

$$\rho_p(w_p - w_a)\frac{da}{dt} = -\rho_{liq} D\left(\frac{\partial w}{\partial r}\right)_{r=a}, \tag{9}$$

where ρ_p and ρ_{liq} are particle and liquid density respectively, and w_p is the mass fraction of the relevant component in the newly growing or dissolving particle (crystal or drop or bubble). Combining Equations (8) and (9), the following is obtained:

$$\frac{da}{dt} = (\rho_{liq}/\rho_p)\frac{D}{\delta}\frac{w_a - w_\infty}{w_p - w_a}, \tag{10}$$

As long as the relevant diffusivity and densities are known, given the initial liquid and particle composition, and knowing how to estimate the interface liquid composition (using the equilibrium condition), the only unknown in calculating the growth or dissolution rate is the effective boundary layer thickness δ.

The effective boundary layer thickness δ is obtained through fluid dynamic relations as follows. The Sherwood number (Sh) is defined as $2a/\delta$ (diameter of the particle divided by the effective boundary layer thickness). Hence, estimating δ becomes the problem of estimating Sh, which for a rising or falling particle at $Re \leq 1$ can be expressed as a function of the Peclet number Pe (Clift *et al*., 1978; Kerr, 1995):

$$Sh = 1 + (1 + Pe)^{1/3}, \tag{11}$$

where $Pe = 2aU/D$ where U is the rising or falling velocity. For $Re \leq 10^5$ Sh can be expressed as a function of both Pe and the Reynolds number Re:

$$Sh = 1 + (1 + Pe)^{1/3}\left(1 + \frac{0.096Re^{1/3}}{1 + 7Re^{-2}}\right), \tag{12}$$

where $Re = 2aU\rho_{liq}/\eta_{liq}$ where ρ_{liq} is liquid density and η_{liq} is the liquid viscosity.

The rising velocity is calculated from Stokes' law for $Re \leq 1$:

$$U = \frac{2ga^2\Delta\rho}{9\eta}, \tag{13}$$

where $\triangle\rho$ is the density difference between the particle and the liquid, and drops and bubbles are assumed to behave as rigid spheres. For $Re \leq 3 \times 10^5$, the velocity U, Reynolds number Re, and drag coefficient C_D must be solved from the following 3 equations:

$$U = \sqrt{\frac{8ga\Delta\rho}{3\rho_{liq}C_D}}, \tag{14}$$

$$Re = 2aU\rho_{liq}/\eta_{liq}, \tag{15}$$

$$C_D = \frac{24}{Re}(1 + 0.15Re^{0.687}) + \frac{0.42}{1 + 42500Re^{-1.16}}. \tag{16}$$

For CO_2 drop dissolution in seawater, Re can be up to 900. Hence, it is necessary to use the theory of Zhang & Xu (2003) to calculate the dissolution rate of CO_2 drops in seawater. The CO_2 concentration in the interface seawater is assumed to be the CO_2 solubility of CO_2 hydrate in seawater (Zhang, 2005). The calculation is done numerically at each depth including the temperature variation with depth. Figure 5 compares the calculated results (Zhang, 2005) with experimental data by Brewer *et al*. (2002), with excellent agreement, verifying the convective

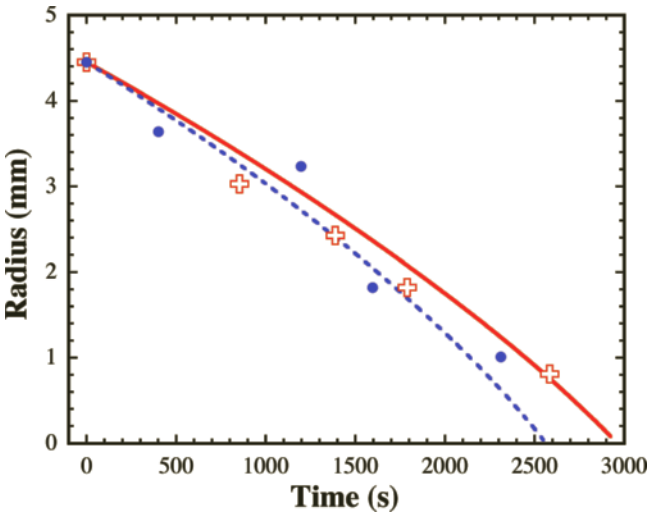

Fig. 5. CO_2 liquid drop dissolution upon rising in seawater. From Zhang (2005) and Zhang & Kling (2006). The points are directly measured data for CO_2 liquid drop dissolution in seawater (Brewer *et al*., 2002). The curves are from the convective dissolution model (Zhang, 2005).

dissolution or growth theory. The success also means that no more experiments are necessary, and CO_2 drop dissolution rate as it rises or falls in seawater in any part of the ocean can be calculated accurately given seawater temperature, depth and salinity, which can be part of a larger program to model the fate of CO_2 in seawater circulation.

One note to the above theory and calculation is about the presence of flow in the ambient fluid, which might well be present in seawater during the experiments of Brewer *et al.* (2002). Because it is the compositional boundary layer that affects the dissolution or growth rate, and the boundary layer thickness is only affected by the relative motion between the particle and the fluid, other fluid motions, even if they entrain the particle, do not affect the boundary layer thickness unless it is so turbulent that it would disturb the thin boundary layer (about 40 μm in the case of CO_2 drop dissolution). For example, Walker & Kiefer (1985) compared dissolution rate of NaCl crystals falling in static water and in turbulent water and found no increase in dissolution rate for the case of turbulent water. Hence, the presence of other flow usually does not affect the convective dissolution or growth rate of a falling or rising particle.

Although the above application is for the dissolution of a single rising CO_2 drop in an infinite reservoir of seawater, the theory can be applied to handle the convective dissolution or growth of many falling or rising particles by allowing the far-field concentration w_∞ in Equations (8) and (10) to vary as long as the particles are separated from each other by a mean distance much larger than the radius. Under such conditions, direct interaction among the particles can be ignored. For example, the continued growth or dissolution of many particles, such as growth of sulfide liquid droplets and monosulfide crystals (which may settle to form sulfide ores), may alter the far-field liquid composition. Therefore, the far-field liquid composition does not have to be the same as the initial liquid composition. By allowing the far-field composition to change, the convective growth or dissolution of many particles separated far from each other can be treated. The far-field composition can be estimated from mass balance, starting from the initial composition, adding the extra mass due to particle dissolution and subtracting the extra mass in the boundary layer.

6. Convective dissolution of halide crystals in water

Kerr (1995) and Zhang & Xu (2003) carried out experiments to examine convective dissolution of falling halide crystals in aqueous solutions to verify their convective dissolution theory. Kerr (1995) added 0.95 wt% of soluble CMC (sodium carboxymethyl cellulose) polymer to water to increase the viscosity of the solution so that the Reynolds number for NaCl falling in the solution is less than 1. It is assumed that the NaCl diffusivity is not changed by the addition of CMC. Zhang & Xu (2003) used pure water as the starting liquid. Figure 6 compares the experimental data (points) and calculation using the theory in Section 5.

Because the solubility of halide in water is very high, halide concentration in the boundary layer varies a lot, from zero to over 20 wt%. This variation leads to some complications, including significant variation of viscosity, diffusivity and density across the boundary layer, and the additional driving force on sinking due to high density in the boundary layer. These complication factors are not included in convective crystal dissolution models in section 5, and hence can cause some errors. On the other hand, for CO_2 drop dissolution into seawater, the CO_2 solubility is small, meaning that none of the complications mentioned here is significant for the case of CO_2 drop dissolution. Thus, the calculated convective halide dissolution curves may deviate from experimental data by about 20% relative (Fig. 6), and are not as good as the prediction for CO_2 drop dissolution (Fig. 5).

7. Convective bubble growth in beer

The theory for the convective growth or dissolution can also be applied to estimate the growth rate of rising bubbles in beer and other bubbly drinks. For beer enthusiasts, the strings of bubbles and the foam head add to the aesthetics of beer. A string of bubbles is formed by discrete release of bubbles from a single nucleation site at some fixed time interval. As discussed by Liger-Belair (2004), nucleation sites are often micrometer-sized fiber particles.

The same equations outlined in section 5 can be used to calculate the growth of a rising spherical bubble in beer, with one exception: volume of bubbles depends also on the pressure (and hence height in a fluid column). That is, one cannot assume a constant density of gases in a bubble and directly calculate da/dt using Equation (10) because a bubble grows due to both additional mass and expansion. Instead, the number of moles of gas M in the bubble is

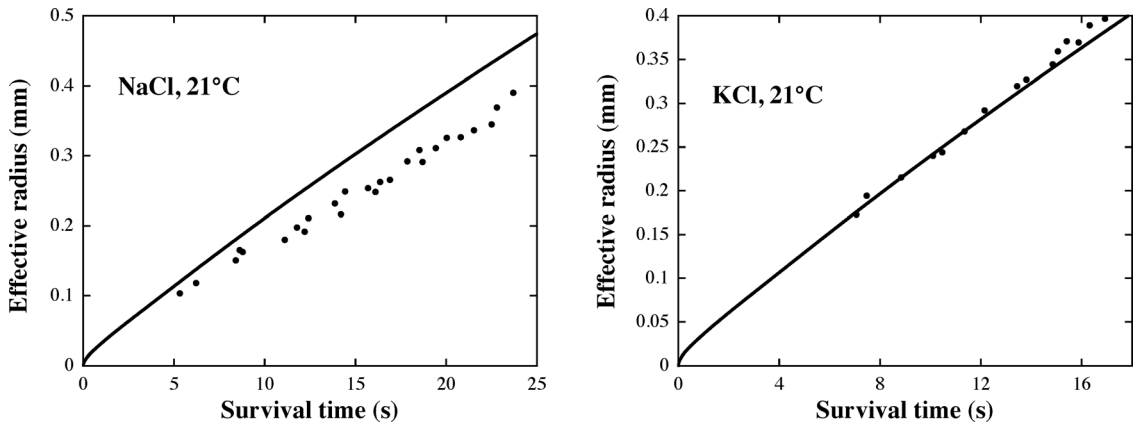

Fig. 6. Halide dissolution: comparison between data (points) and calculation (curves). From Zhang & Xu (2003).

obtained by calculating the mass gain of the bubble (Zhang & Xu, 2008):

$$\frac{\mathrm{d}M}{\mathrm{d}t} = 4\pi a^2 D\left(\frac{\partial C}{\partial r}\right)_{r=a} = 4\pi a^2 D\frac{C_\infty - C_a}{\delta}, \qquad (17)$$

where M is total moles of gas in the bubble and C is the concentration (in mol/m^3) of the gas component in the liquid. Integration of the above equation leads to new M in the bubble, and then new bubble radius a can be calculated from the new M and the new pressure P given the equation of state (such as the ideal gas law). For bubble growth, the expansion upon rising adds to the growth due to mass increase. For bubble dissolution, the expansion leads to bubble size increase as a bubble rises but mass loss leads to bubble size decrease. Under the appropriate conditions, it is even possible for a dissolving bubble to become larger as it rises (Zhang, 2003).

Shafer & Zare (1991) measured the size of bubbles in a bubble string in beer. Assuming all bubbles are of the same size when released from the nucleation site, the data show how rapidly a bubble grows as it rises in beer. Shafer & Zare (1991) successfully calculated the rising velocity and trajectory of the bubbles given their size, but used a simple linear function to fit the bubble size. For accurate calculation of the bubble growth rate, it is necessary to guess the temperature during the experiment and the initial CO_2 content in the glass of beer, which has lost some of the initial CO_2 as beer is poured into the glass. Zhang & Xu (2008) found that by assuming a temperature of 9°C and an initial CO_2 content corresponding to a pressure of 1.63 bars (rather than about 2 bars of CO_2 for completely undegassed beer), the calculated growth curve matches experimental data within error (Fig. 7).

8. Mineral dissolution in silicate melt

For understanding crystal growth and dissolution kinetics, experimental studies often focus on crystal dissolution rather than crystal growth because crystal dissolution is easier to control experimentally. For example, crystal growth requires the melt to be supersaturated with a mineral. Under such conditions, it is impossible to control where and how many new crystals would form in the experimental charge, and these new crystals might disturb the growth of existing crystals. On the other hand, in dissolution experiments, the melt is undersaturated. Dissolution only occurs at the interface between the initially present crystal and melt, meaning that no additional complications need to be considered. Hence, most recent experiments aimed at understanding crystal dissolution or growth are crystal dissolution experiments (*e.g.*, Watson, 1982; Zhang *et al.*, 1989; Kerr, 1995; Shaw, 2000, 2004; Chen & Zhang, 2008, 2009).

Mineral dissolution in a magma chamber is often accompanied by the fall or rise of the mineral, meaning that it is necessary to use the convective model. With the above theory on convective particle dissolution (Section 5), the critical parameters in estimating convective mineral dissolution rate are: melt viscosity, solubility and diffusivity of the relevant component, and initial compositional and T-P conditions. Solubility and diffusivity of the relevant component can be obtained from diffusive crystal dissolution experiments. Because one-dimensional diffusive crystal dissolution experiments are more convenient to conduct and interpret, authors have used such experiments to obtain diffusivity and solubility, so as to predict three-dimensional convective dissolution rates (Chen & Zhang, 2008, 2009). The other key parameter, viscosity, is often calculated using recent viscosity models for all silicate melts (*e.g.*, Hui & Zhang, 2007).

Previously, convective particle dissolution theory was applied to model convective mineral dissolution without direct verification (Kerr, 1995; Chen & Zhang, 2008, 2009). One complexity is the effect of viscosity and diffusivity variation across the boundary layer, which is not accounted for in the convective dissolution or growth theory. Kerr (1995) estimated the dissolution time for a given size of felsic crystals. Chen & Zhang (2008) estimated the dissolution time of olivine in a MORB melt given temperature, pressure, and initial size. Chen & Zhang (2009) did the same for diopside dissolution in a basaltic melt. These results have not been verified yet.

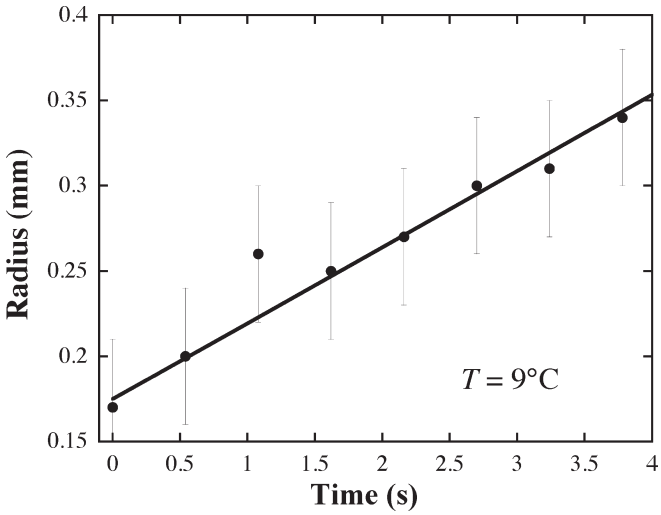

Fig. 7. CO_2 bubble growth in beer: comparison between data and calculation. From Zhang & Xu (2008).

Although experiments on convective crystal dissolution in high-temperature silicate melt are difficult, Quetscher *et al*. (2012) have been making progress and developed an experimental method to obtain convective crystal dissolution rate in silicate melts. The work is ongoing and will provide much needed critical information to verify or improve the applicability of convective particle dissolution to crystal dissolution in silicate melts.

9. Summary

Significant progress has been made in the last 20 years on quantitatively predicting particle dissolution or growth rates in a liquid. Both diffusive and convective particle dissolution or growth rates can now be calculated without free fitting parameters. It is hoped that the theories will be applied to solve other critical problems in various branches of Earth and planetary sciences, such as bubble growth and degassing in lunar melts, sulfide ore formation, and magma ocean evolution kinetics and dynamics.

Acknowledgements: This review is based on a keynote lecture delivered at the European Mineralogy, Petrology and Geochemistry (EMPG2012) Meeting in Kiel, Germany. I thank Harald Behrens for the invitation, and two anonymous reviewers for constructive comments. This work is supported in part by the US NSF (grants EAR-0838127 and EAR-1019440) and NASA (grant NNX10AH74G).

References

Acosta-Vigil, A., London, D., Dewers, T.A., Morgan VI, G.B. (2002): Dissolution of corundum and andalusite in H_2O-saturated haplogranitic melts at 800°C and 200 MPa: constraints on diffusivities and the generation of peraluminous melts. *J. Petrol.*, **43**, 1885–1908.

Acosta-Vigil, A., London, D., Morgan VI, G.B., Dewars, T.A. (2006): Dissolution of quartz, albite, and orthoclase in H_2O-saturated haplogranitic melt at 800°C and 200 MPa: diffusive transport properties of granitic melts at crustal anatectic conditions. *J. Petrol.*, **47**, 231–254.

Angus, S., Armstrong, B., de Reuck, K.M. (1976): International thermodynamics tables of the fluid state: carbon dioxide. Pergamon Press, Oxford, 385 p.

Baker, D.R. & Moretti, R. (2011): Modeling the solubility of sulfur in magmas: a 50-year old geochemical challenge. *Rev. Mineral. Geochem.*, **73**, 167–213.

Barnes, S.J. (2007): Cotectic precipitation of olivine and sulfide liquid from komatiite magma and the origin of komatiite-hosted disseminated nickel sulfide mineralization at Mount Keith and Yakabindie, western Australia. *Econ. Geol.*, **102**, 299–304.

Beermann, O., Botcharnikov, R.E., Holtz, F., Diedrich, O., Nowak, M. (2011): Temperature dependence of sulfide and sulfate solubility in olivine-saturated basaltic magmas. *Geochim. Cosmochim. Acta*, **75**, 7612–7631.

Berner, R.A. (1978): Rate control of mineral dissolution under Earth surface conditions. *Am. J. Sci.*, **278**, 1235–1252.

Blank, J.G., Stolper, E.M., Carroll, M.R. (1993): Solubilities of carbon dioxide and water in rhyolitic melt at 850°C and 750 bars. *Earth Planet. Sci. Lett.*, **119**, 27–36.

Blower, J.D., Mader, H.M., Wilson, S.D.R. (2001): Coupling of viscous and diffusive controls on bubble growth during explosive volcanic eruptions. *Earth Planet. Sci. Lett.*, **193**, 47–56.

Bockrath, C., Ballhaus, C., Holzheid, A. (2004): Fractionation of the platinum-group elements during mantle melting. *Science*, **305**, 1951–1953.

Botcharnikov, R.E., Linnen, R.L., Wilke, M., Holtz, F., Jugo, P.J., Berndt, J. (2011): High gold concentrations in sulfide-bearing magma under oxidizing conditions. *Nature Geosci.*, **4**, 112–115.

Bowen, N.L. (1914): The ternary system: diopside-forsterite-silica. *Am. J. Sci.*, **38**, 207–264.

Brewer, P.G., Peltzer, E.T., Friedrich, G., Rehder, G. (2002): Experimental determination of the fate of rising CO_2 droplets in seawater. *Environ. Sci. Technol.*, **36**, 5441–5446.

Buchanan, D.L. & Nolan, J. (1979): Solubility of sulfur and sulfide immiscibility in synthetic tholeiitic melts and their relevance to Bushveld-Complex rocks: *Can. Mineral*, **17**, 483–494.

Carroll, M.R. & Rutherford, M.J. (1987): The stability of igneous anhydrite: experimental results and implications for sulfur behavior in the 1982 El Chichon trachyandesite and other volved magmas. *J. Petrol.*, **28**, 781–801.

Carslaw, H.S. & Jaeger, J.C. (1959): Conduction of Heat in Solids. Clarendon Press, Oxford, 510 p.

Chen, Y. & Zhang, Y. (2008): Olivine dissolution in basaltic melt. *Geochim. Cosmochim. Acta*, **72**, 4756–4777.

—, — (2009): Clinopyroxene dissolution in basaltic melt. *Geochim. Cosmochim. Acta*, **73**, 5730–5747.

Clift, R., Grace, J.R., Weber, M.E. (1978): Bubbles, drops, and particles. Academic Press, New York, NY, 380 p.

Cussler, E.L. (1997): Diffusion: mass transfer in fluid systems. Cambridge University Press, Cambridge, England, 580 p.

Delaney, J.R. & Karsten, J.L. (1981): Ion microprobe studies of water in silicate melts: concentration-dependent water diffusion in obsidian. *Earth Planet. Sci. Lett.*, **52**, 191–202.

Dingwell, D.B., Harris, D.M., Scarfe, C.M. (1984): The solubility of H_2O in melts in the system SiO_2-Al_2O_3-Na_2O-K_2O at 1 to 2 kbars. *J. Geol.*, **92**, 387–395.

Epstein, P.S. & Plesset, M.S. (1950): On the stability of gas bubbles in liquid-gas solutions. *J. Chem. Phys.*, **18**, 1505–1509.

Gaetani, G.A. & Grove, T.L. (1997): Partitioning of moderately siderophile elements among olivine, silicate melt, and sulfide melt: constraints on core formation in the Earth and Mars: *Geochim. Cosmochim. Acta*, **61**, 1829–1846.

Gardner, J.E. (2007): Heterogeneous bubble nucleation in highly viscous silicate melts during instantaneous decompression from high pressure. *Chem. Geol.*, **236**, 1–12.

Gardner, J.E. & Denis, M.H. (2004): Heterogeneous bubble nucleation on Fe-Ti oxide crystals in high-silica rhyolitic melts. *Geochim. Cosmochim. Acta*, **68**, 3587–3597.

Gardner, J.E., Hilton, M., Carroll, M.R. (1999): Experimental constraints on degassing of magma: isothermal bubble growth during continuous decompression from high pressure. *Earth Planet. Sci. Lett.*, **168**, 201–218.

—, —, — (2000): Bubble growth in highly viscous silicate melts during continuous decompression from high pressure. *Geochim. Cosmochim. Acta*, **64**, 1473–1483.

Ghiorso, M.S., Hirschmann, M.M., Reiners, P.W., Kress, V.C. (2002): The pMELTS: A revision of MELTS for improved calculation of phase relations and major element partitioning related to partial melting of the mantle to 3 GPa: *Geochem. Geophys. Geosys.*, **3**, U1–U36.

Goranson, R.W. (1938): Silicate-water systems: phase equilibria in the $NaAlSi_3O_8$-H_2O and $KAlSi_3O_8$-H_2O systems at high temperatures and pressures. *Am. J. Sci.*, **35-A**, 71–91.

Harrison, T.M. & Watson, E.B. (1983): Kinetics of zircon dissolution and zirconium diffusion in granitic melts of variable water content. *Contrib. Mineral. Petrol.*, **84**, 66–72.

Haughton, D.R., Roeder, P.L., Skinner, B.J. 1974: Solubility of sulfur in mafic magmas. *Econ. Geol.*, **69**, 451–467.

Hess, K. & Dingwell, D.B. (1996): Viscosities of hydrous leucogranitic melts: a non-Arrhenian model. *Am. Mineral.*, **81**, 1297–1300.

Holtz, F., Behrens, H., Dingwell, D.B., Taylor, R.P. (1992): Water solubility in aluminosilicate melts of haplogranite composition at 2 kbar. *Chem. Geol.*, **96**, 289–302.

Holtz, F., Behrens, H., Dingwell, D.B., Johannes, W. (1995): H_2O solubility in haplogranitic melts: compositional, pressure, and temperature dependence. *Am. Mineral.*, **80**, 94–108.

Holzheid, A. (2010): Separation of sulfide melt droplets in sulfur saturated silicate liquids. *Chem. Geol.*, **274**, 127–135.

Holzheid, A. & Grove, T.L. (2002): Sulfur saturation limits in silicate melts and their implications for core formation scenarios for terrestrial planets. *Am. Mineral.*, **87**, 227–237.

Hui, H. & Zhang, Y. (2007): Toward a general viscosity equation for natural anhydrous and hydrous silicate melts. *Geochim. Cosmochim. Acta*, **71**, 403–416.

Hui, H., Zhang, Y., Xu, Z., Del Gaudio, P., Behrens, H. (2009): Pressure dependence of viscosity of rhyolitic melts. *Geochim. Cosmochim. Acta*, **73**, 3680–3693.

Hurwitz, S. & Navon, O. (1994): Bubble nucleation in rhyolitic melts: experiments at high pressure, temperature, and water content. *Earth Planet. Sci. Lett.*, **122**, 267–280.

Ihinger, P.D. 1991, An experimental study of the interaction of water with granitic melt [Ph.D. thesis], California Institute of Technology.

Jugo, P.J. 2009: Sulfur content at sulfide saturation in oxidized magmas. *Geology*, **37**, 415–418.

Jugo, P.J., Luth, R.W., Richards, J.P. (2005a): Experimental data on the speciation of sulfur as a function of oxygen fugacity in basaltic melts. *Geochim. Cosmochim. Acta*, **69**, 497–503.

—, —, — (2005b): An experimental study of the sulfur content in basaltic melts saturated with immiscible sulfide or sulfate liquids at 1300°C ajd 1.0 GPa. *J. Petrol.*, **46**, 783–798.

Kadik, A.A., Lukanin, O.A., Lebedev, Y.B., Korovushkina, E.Y. (1972): Solubility of H_2O and CO_2 in granite and basalt melts at high pressures. *Geochem. Int.*, **9**, 1041–1050.

Kerr, R.C. (1995): Convective crystal dissolution. *Contrib. Mineral. Petrol.*, **121**, 237–246.

Khitarov, N.I. & Kadik, A.A. (1973): Water and carbon dioxide in magmatic melts and peculiarities of the melting process. *Contrib. Mineral. Petrol.*, **41**, 205–215.

Kress, V.C., Greene, L.E., Ortiz, M.D., Mioduszewski, L. (2008): Thermochemistry of sulfide liquids IV: density measurements and the thermodynamics of O-S-Fe-Ni-Cu liquid at low to moderate pressures. *Contrib. Mineral. Petrol.*, **156**, 785–797.

Lange, R.A. & Carmichael, I.S.E. (1990): Thermodynamic properties of silicate liquids with an emphasis on density, thermal expansion and compressibility. *Rev. Mineral.*, **24**, 25–64.

Larsen, J.F. (2008): Heterogeneous bubble nucleation and disequilibrium H_2O exsolution in Vesuvius K-phonolite melts. *J. Volcanol. Geotherm. Res.*, **175**, 278–288.

Larsen, J.F. & Gardner, J.E. (2004): Experimental study of water degassing from phonolite melts: implications for volatile oversaturation during magmatic ascent. *J. Volcanol. Geotherm. Res.*, **134**, 109–124.

Lensky, N.G., Navon, O., Lyakhovsky, V. (2004): Bubble growth during decompression of magma: experimental and theoretical investigations. *J. Volcanol. Geotherm. Res.*, **129**, 7–22.

Liang, Y. (1999): Diffusive dissolution in ternary systems: analysis with applications to quartz and quartzite dissolution in molten silicates. *Geochim. Cosmochim. Acta*, **63**, 3983–3995.

— (2000): Dissolution in molten silicates: effects of solid solution. *Geochim. Cosmochim. Acta*, **64**, 1617–1627.

Liger-Belair, G. (2002): Physicochemical approaches to the effervescence in Champagne wines. *Ann. Phys. (Paris)*, **27**, 1–106.

Liu, Y., Samaha, N.T., Baker, D.R. (2007): Sulfur concentration at sulfide saturation (SCSS) in magmatic silicate melts. *Geochim. Cosmochim. Acta*, **71**, 1783–1799.

Liu, Y. & Zhang, Y. (2000): Bubble growth in rhyolitic melt. *Earth Planet. Sci. Lett.*, **181**, 251–264.

Luhr, J.F. (1990): Experimental phase relations of water- and sulfur-saturated arc magmas and the 1982 eruptions of El Chichon volcano. *J. Petrol.*, **31**, 1071–1114.

Lyakhovsky, V., Hurwitz, S., Navon, O. (1996): Bubble growth in rhyolitic melts: experimental and numerical investigation. *Bull. Volcanol.*, **58**, 19–32.

Mavrogenes, J.A. & O'Neill, H.S.C. (1999): The relative effects of pressure, temperature and oxygen fugacity on the solubility of sulfide in mafic magmas. *Geochim. Cosmochim. Acta*, **63**, 1173–1180.

Moore, G., Vennemann, T., Carmichael, I.S.E. (1995): The solubility of water in natural silicate melts to 2 kilobars. *Geology*, **23**, 1009–1102.

—, —, — (1998): An empirical model for the solubility of H_2O in magmas to 3 kilobars. *Am. Mineral.*, **83**, 36–42.

Moretti, R. & Baker, D.R. (2008): Modeling the interplay of fO_2 and fS_2 along the FeS-silicate melt equilibrium. *Chem. Geol.*, **256**, 286–298.

Moretti, R. & Ottonello, G. (2005): Solubility and speciation of sulfur in silicate melts: the Conjugated Toop-Samis-Flood-Grjotheim (CTSFG) model. *Geochim. Cosmochim. Acta*, **69**, 801–823.

Morgan, Z., Liang, Y., Hess, P.C. (2006): An experimental study of anorthosite dissolution in lunar picritic magmas: implications for crustal assimilation processes. *Geochim. Cosmochim. Acta*, **70**, 3477–3491.

Naldrett, A.J. (1969): A portion of system Fe-S-O between 900 and 1080°C and its application to sulfide ore magmas. *J. Petrol.*, **10**, 171–201.

Navon, O., Chekhmir, A., Lyakhovsky, V. (1998): Bubble growth in highly viscous melts: theory, experiments, and autoexplosivity of dome lavas. *Earth Planet. Sci. Lett.*, **160**, 763–776.

Ni, H. & Zhang, Y. (2008): H_2O diffusion models in rhyolitic melt with new high pressure data. *Chem. Geol.*, **250**, 68–78.

Ochs, F.A. & Lange, R.A. (1999): The density of hydrous magmatic liquids. *Science*, **283**, 1314–1317.

O'Neill, H.S.C. & Mavrogenes, J.A. (2002): The sulfide capacity and the sulfur content at sulfide saturation of silicate melts at 1400°C and 1 bar. *J. Petrol.*, **43**, 1049–1087.

Peach, C.L. & Mathez, E.A. (1993): Sulfide melt-silicate melt distribution coefficients for nickel and iron and implications for the distribution of other chalcophile elements. *Geochim. Cosmochim. Acta*, **57**, 3013–3021.

Proussevitch, A.A. & Sahagian, D.L. (1998): Dynamics and energetics of bubble growth in magmas: analytical formulation and numerical modeling. *J. Geophys. Res.*, **103**, 18223–18251.

Proussevitch, A.A., Sahagian, D.L., Anderson, A.T. (1993): Dynamics of diffusive bubble growth in magmas: isothermal case. *J. Geophys. Res.*, **98**, 22283–22307.

Quetscher, A., Behrens, H., Zhang, Y. 2012, Testing of crystal dissolution theory in silicate melts, 14th Experimental Mineralogy Petrology Geochemistry: Kiel, Germany.

Scriven, L.E. (1959): On the dynamics of phase growth. *Chem. Eng. Sci.*, **10**, 1–13.

Shafer, N.E. & Zare, R.N. (1991): Through a beer glass darkly. *Phys. Today*, **44**, 48–52.

Shaw, H.R. (1963): Obsidian-H_2O viscosities at 1000 and 2000 bars in the temperature range 700° to 900°C. *J. Geophys. Res.*, **68**, 6337–6343.

— (1972): Viscosities of magmatic silicate liquids: an empirical method of prediction. *Am. J. Sci.*, **272**, 870–893.

— (1974): Diffusion of H_2O in granitic liquids, I: experimental data; II: mass transfer in magma chambers. *in* ''Geochemical Transport and Kinetics'', A.W. Hofmann, B.J. Giletti, H.S. Yoder, R.A. Yund, eds. Carnegie Institution of Washington Publ. **634**, Washington, DC, 139–170.

Shaw, C.S.J. (2000): The effect of experiment geometry on the mechanism and rate of dissolution of quartz in basanite at 0.5 GPa and 1350°C. *Contrib. Mineral. Petrol.*, **139**, 509–525.

— (2004): Mechanisms and rates of quartz dissolution in melts in the CMAS (CaO-MgO-Al_2O_3-SiO_2) system. *Contrib. Mineral. Petrol.*, **148**, 180–200.

— (2006): Effects of melt viscosity and silica activity on the rate and mechanism of quartz dissolution in the melts of the CMAS and CAS systems. *Contrib. Mineral. Petrol.*, **151**, 665–680.

Shima, H. & Naldrett, A.J. (1975): Solubility of sulfur in an ultramafic melt and the relevance of the system Fe-S-O. *Econ. Geol.*, **70**, 960–967.

Silver, L., Ihinger, P.D., Stolper, E. (1990): The influence of bulk composition on the speciation of water in silicate glasses. *Contrib. Mineral. Petrol.*, **104**, 142–162.

Sparks, R.S.J. (1978): The dynamics of bubble formation and growth in magmas: a review and analysis. *J. Volcanol. Geotherm. Res.*, **3**, 1–37.

Tsuchiyama, A. & Takahashi, E. (1983): Melting kinetics of a plagioclase feldspar. *Contrib. Mineral. Petrol.*, **84**, 345–354.

Tuttle, O.F. & Bowen, N.L. (1958): Origin of granite in the light of experimental studies in the system $NaAlSi_3O_8$-$KAlSi_3O_8$-SiO_2-H_2O: memoirs. *Geol. Soc. Am.*, **74**, 1–153.

Walker, D. & Kiefer, W.S. (1985): Xenolith digestion in large magma bodies. *J. Geophys. Res.*, **90**, C585–C590.

Walker, D. & Mullins, O. (1981): Surface tension of natural silicate melts from 1200°-1500°C and implications for melt structure. *Contrib. Mineral. Petrol.*, **76**, 455–462.

Wang, P.K. & Pruppacher, H.R. (1977): Acceleration to terminal velocity of cloud and raindrops. *J. Appl. Meteor.*, **16**, 275–280.

Watson, E.B. (1982): Basalt contamination by continental crust: some experiments and models. *Contrib. Mineral. Petrol.*, **80**, 73–87.

Zhang, Y. (1999a): A criterion for the fragmentation of bubbly magma based on brittle failure theory. *Nature*, **402**, 648–650.

— (1999b): H_2O in rhyolitic glasses and melts: measurement, speciation, solubility, and diffusion. *Rev. Geophys.*, **37**, 493–516.

— (2003): Methane escape from gas hydrate systems in marine environment, and methane-driven oceanic eruptions. *Geophys. Res. Lett.*, **30**, 1398, doi:10.1029/2002GL016658

— (2005b): Fate of rising CO_2 droplets in seawater. *Environ. Sci. Technol.*, **39**, 7719–7724.

— (2008): Geochemical kinetics. Princeton University Press, Princeton, NJ, 656 p.

Zhang, Y. & Behrens, H. (2000): H_2O diffusion in rhyolitic melts and glasses. *Chem. Geol.*, **169**, 243–262.

Zhang, Y. & Kling, G.W. (2006): Dynamics of lake eruptions and possible ocean eruptions. *Annu. Rev. Earth Planet. Sci.*, **34**, 293–324.

Zhang, Y. & Stolper, E.M. (1991): Water diffusion in basaltic melts. *Nature*, **351**, 306–309.

Zhang, Y. & Xu, Z. (2003): Kinetics of convective crystal dissolution and melting, with applications to methane hydrate dissolution and dissociation in seawater. *Earth Planet. Sci. Lett.*, **213**, 133–148.

—, — (2008): Fizzics'' of bubble growth in beer and champagne. *Elements*, **4**, 47–49.

Zhang, Y., Walker, D., Lesher, C.E. (1989): Diffusive crystal dissolution. *Contrib. Mineral. Petrol.*, **102**, 492–513.

Zhang, Y., Stolper, E.M., Wasserburg, G.J. (1991a): Diffusion of water in rhyolitic glasses. *Geochim. Cosmochim. Acta*, **55**, 441–456.

—, —, — (1991b): Diffusion of a multi-species component and its role in the diffusion of water and oxygen in silicates. *Earth Planet. Sci. Lett.*, **103**, 228–240.

Zhang, Y., Xu, Z., Liu, Y. (2003): Viscosity of hydrous rhyolitic melts inferred from kinetic experiments, and a new viscosity model. *Am. Mineral.*, **88**, 1741–1752.

Zhang, Y., Xu, Z., Zhu, M., Wang, H. (2007): Silicate melt properties and volcanic eruptions. *Rev. Geophys.*, **45**, RG4004.

Received 13 June 2012
Modified version received 17 February 2013
Accepted 18 February 2013